Int J Adv Manuf Technol (2017) 93:1399–1413
DOI 10.1007/s00170-017-0599-0

ORIGINAL ARTICLE

A study on the different finite element approaches for laser cutting of aluminum alloy sheet

S. Peirovi[1] · M. Pourasghar[2] · A. Farokhi Nejad[3] · M. A. Hassan[1]

Received: 9 January 2017 / Accepted: 31 May 2017 / Published online: 13 June 2017

Abstract The effectiveness of finite element simulation techniques for laser cutting of 1.2-mm-thick aluminium sheets has been studied. Lagrangian and Arbitrary Lagrangian-Eulerian techniques were used to model and simulate laser cutting process. The reliability of finite element results were evaluated by general energy balance analysis and experimental results. Temperature and stress distribution along with heat-affected zone were predicted during the laser-induced process in line with experimental conditions under ABAQUS finite element code. Heat transfer analysis relying on thermal loading was employed to reach the best efficiency. By using field-emission scanning electron microscope, morphological, structural, and elemental changes in the cutting sections were analyzed along with the X-ray diffraction technique. Obtained stress and heat-affected zone are highly dependent on the element type as well as numerical method. Both numerical method, ALE and Lagrangian, are compared to each other in terms of power absorption, cut surface morphology, and cutting efficiency. The results show that ALE method is in good agreement with experimental data.

Keywords Laser cutting · Aluminum sheets · Finite element method · General energy balance · Thermal stress

1 Introduction

In today's competitive industrial environment, the vast majority of manufacturing firms are utilizing technological methods to enhance workplace productivity. In between, the laser cutting has turned to be one of the effective methods for cutting sheet metals due to its flexibility and time consuming. Moreover, unlike conventional cutting methods, laser cutting offers significant advantages in terms of productivity where it could be performed by inducing the high intensity laser beam over small region of material [1, 2]. Considerable research studies indicate that great variety of existing mass production in automotive, aerospace, and computer industry relies on aluminum sheets [3].

The laser cutting as a powerful method could localize temperature by inducing temperature gradient along the cutting path. Some studies have conducted the effects of temperature gradient and thermal stress in laser cutting process. Experimental results in these research indicate that power density, cutting speed, and laser pulse, as significant control factors, have direct effects on microstructural characteristics, grain morphology, kerf dimension, and surface finishing [4–6].

Stournaras et al. [7] were carried out a statistical study on the effect of significant parameters on laser cutting process . Also, Wang et al. [8] have found that, in laser cutting process, the quality of surface in cutting section is considerably affected by the size of spherical particle under various melting ratio.

Several theoretical studies have evaluated the effect of temperature and stress in laser cutting in order to enhance

✉ A. Farokhi Nejad
ali.farokhi@polito.it

[1] Department of Mechanical Engineering, University of Malaya, 50603 Kuala Lumpur, Malaysia

[2] Automatic Control Department, Universitat Politècnica de Catalunya, C/. Llorens i Artigas 4-6, 08028 Barcelona, Spain

[3] Dipartimento di ing. Meccanica e aerospaziale, Poletecnico di Torino Corso Duca degli Abruzzi 24, 10139 Torino, Italy

the process. The first mathematical model that has proposed by Antony et al. [9] investigates the Gaussian power distribution for laser heating, as a constant source of moving heat, as well as study on the laser characteristics during the heating or melting phenomena. Furthermore, a two-dimensional model with coordinate transformation for modeling the laser motion was proposed by Pandey [10]. Dubey [11] has presented an empirical model to optimize the kerf taper and kerf variation during the laser cutting process of duralumin alloy. Sheng and Joshi [12] have developed a numerical model to estimate the heat-affected zone (HAZ) for cutting the steel sheet . Yilbas et al. (a) [13] have validated a numerical model through experiment for investigating the small variation of temperature through the thickness of zirconia tile specimen. In other studies, Yilbas et al. (b) [14] have performed a three dimensional Finite Element (FE) Model to study thermal stress during the laser cutting of the rectangular path on the aluminum alloy specimen. They have found that the thermal stress concentration would be occurred at the sharp edge of specimen. In addition, related FE studies have been carried out to model the effect of transient temperature and residual stress during the laser cutting [15, 16].

The recent research have utilized only the Lagrangian element to simulate the laser cutting process while fixed FE formulation was applied on all space or material domain [17–19]. The result of the Lagrangian method shows the high dependency on the size and density of elements over the laser induced region. On the other hand, the Arbitrary Lagrangian-Eulerian (ALE) formulation can reduce specific problems which relates to the FE simulation with traditional Lagrangian-based formulation. The computational mesh moves arbitrarily inside the domain when the ALE method is utilized. To optimize the element shape, the mesh of the boundaries in the domain moves along with materials to precisely follow the boundaries and interfaces of different materials region. Meanwhile, ALE method reduces the formulation of either Lagrangian method by equating the mesh motion to material motion or Eulerian method by fixing the domain [20]. This advantage can be considered as an effective technique to perform comprehensive simulation for different applications including heat transfer, fluid flow and especially in metal manufacturing, e.g., metal forming, metal casting and metal cutting. Although, the FE method applied on many research for particular purposes such as temperature and stress distribution, less attention has been paid to the type of element and the FE solution techniques.

In the present study, the laser cutting of aluminum sheets based on two different FE formulations:Lagrangian and ALE methods are simulated while temperature and stress distribution are predicted. In the simulation, the FE results precisely demonstrate the residual stress and kerf width dimensions after cutting process. Moreover, the FE results and experimental findings are compared to distinguish the reliable method.

2 Heat transfer problem

2.1 Thermal loads and assumptions

From heat transfer point of view the beam absorption, refraction, heat conduction and heat loss by radiation and/or convection from the material surface are some of the laser induction effects. The general types of thermal loads can be applied on the fully coupled temperature-displacement analysis, (i) concentrated heat flux prescribed at a point, (ii) distributed heat flux on area, (iii) body heat flux per unit volume, (iv) boundary convection, and (v) boundary radiation. The nature of standard procedure in normal process of laser cutting is thermal. In order to derive the mathematical model, some assumptions are made as below:

- The isotropic material used in the model has constant optical and thermal properties.
- Material travels at a relatively constant speed.
- The laser beam type is Gaussian with a constant diameter.
- Change of phase from solid to gas happens in one step.
- The specimen was homogenous and isotropic.
- The transparent material that is evaporated does not have interference with incident beam.

2.2 Heat transfer equation

The Fourier equation for thermal transfer in the process of laser heating is as follow:

$$\rho \frac{DE}{Dt} = (\nabla(k\nabla T)), \tag{1}$$

where k is the thermal conductivity, ρ is the density of material and E is the energy gain of substrate material. If there is a dynamic heat source along with Y-axis of the sheet with a constant speed U, the energy gain will be

$$\rho \frac{DE}{Dt} = \rho \frac{\partial(C_p T)}{\partial t} + \rho U \frac{(\partial(C_p T))}{\partial y}. \tag{2}$$

Combining (1) and (2) yields

$$\rho \frac{(\partial(C_p T))}{Dt} = (\nabla(k\nabla T)) + \rho U \frac{(\partial(C_p T))}{\partial y}, \tag{3}$$

where C_p is the specific heat which is related to the internal gain of energy. The equation of heat transfer for the laser heating is as follow:

$$\rho \frac{\partial(H(T))}{\partial t} = (\nabla(k(T)\nabla T)) + \rho U \frac{(\partial(C_p(T)T))}{\partial y}, \tag{4}$$

where k is temperature dependent thermal conductivities, U as the moving heat source velocity, ρ as the density and H

is the temperature dependent enthalpy. For this problem, the boundary conditions can be: At the top surface of the work-piece alongside the cutting section where the boundary is considered as

$$\frac{\partial T}{\partial z} = \frac{h_f}{k}(T_s - T_{amb}) + \frac{\epsilon\sigma}{k}\left(T_s^4 - T_{amb}^4\right), \tag{5}$$

where h_f is the heat transfer coefficient along of the assisting gas, and T_s and T_{amb} are the surface temperature and ambient temperature, respectively, ϵ is emissivity, σ is known as Stefan-Boltzmann constant and k is the thermal conductivity.

And at the bottom surface we have

$$\frac{\partial T}{\partial z} = \frac{h}{k}(T_s - T_{amb}) + \frac{\epsilon\sigma}{k}\left(T_s^4 - T_{amb}^4\right), \tag{6}$$

where h is the heat transfer coefficient along of natural convection. Consequently, proper temporal and spatial discretization will be available. At the boundaries which are far away (at the edge of the plate), the temperature is assumed to be constant (T=293 K), i.e.,

$$x = \infty; y = \infty; z = t_h. \tag{7}$$

3 Thermo-mechanical coupling problem

In general, the physical description of the thermo mechanical problem by the first law of thermo-dynamics and the balance of momentum with the constitutive laws leads to a system of field equations where the temperature field is unknown and the mechanical equation with the displacement field can be determined as known variables. However, in terms of mechanics and thermodynamics, the governing equations are considered as temperature dependent equations. According to the first thermodynamics law, the change of internal and kinetic energy of any portion of a body equals to the rate of work that is done on that portion as well as the rate of heat supply and heat flow across the boundary. Thus, local form of the first law of thermodynamics is

$$\rho\dot{e} + \nabla q = \sigma : d + \rho r, \tag{8}$$

where q is the vector of heat flux, $\dot{e}$ is the internal energy per unit mass, d is the rate of deformation tensor and the heat supply per unit mass is shown by r. The d can be found using derivatives of Lie as follows:

$$d = L_v e = 1/2 L_v g, \tag{9}$$

where g is the spatial metric tensor and e is the Eulerian strain tensor also L_v represents the Lie derivative. The e may be expanded in term of the deformation gradient F:

$$e = \frac{1}{2}\left(g - \left(F^{-T}F^{-1}\right)^b\right), \tag{10}$$

where b denotes lowering of all indices. This system of equation is strongly coupled, i.e., the mechanical equation is a function of the temperature field and the thermal equation is a function of the displacement field.

4 Methodology

The finite element method is used to solve (4) under the boundary and initial conditions given by Eqs. 5, 6 and 7. Two different heat flux distributions: Element-based distributed surface fluxes (on element faces) or body fluxes (flux per unit volume) are existed [21]. For surface fluxes, it must identify the face of the element upon which the flux is prescribed in the flux label. The DFLUX user subroutine in ABAQUS is used for the numerical solution to develop stress and thermal field around the cutting zone. First, the laser beam position is determined based on the time of scanning (t). Afterwards, the heat ux (Q) is computed at each integration point. As solidification has slight strain, in this work, the small strain is assumed [22]. To calculate the overall strain rate, the following elastic-viscoelastic model is used [23].

$$\dot{\epsilon} = \dot{\epsilon_{el}} + \dot{\epsilon_{ie}} + \dot{\epsilon_{th}}, \tag{11}$$

where $\dot{\epsilon_{th}}$, $\dot{\epsilon_{ie}}$ and $\dot{\epsilon_{el}}$ are the thermal, inelastic and elastic strain rate tensors, respectively. The volume variations associated with the temperature increment ΔT result in the incremental thermal strain, which can be determined by the thermal analysis. It is generally considered in analyses with the temperature dependent thermal expansion coefficient $\alpha(T)$. To calculate the thermal strain in FE model, the backward difference method is used at every integration point. The numerical solution of the thermo-mechanical problem in general depends on the type of the heat flow and steady state, or time variation condition. In the case of transient state, which is complicated, staggered methods are favoured. As such, the problem can be iteratively solved with constant temperature, the corresponding displacement is remained after getting convergence. In laser cutting process material are used with inelastic and large deformation behavior. The behavior of these materials is characterized by small elastic, thermal strains and large inelastic, i.e., plastic strains [24]. Due to the non-uniform temperature distribution, the plastic deformation is varying with the location. However, it could be effected by the heat conduction of the structure from thermal boundary condition. Due to the temperature dependency of the material, the yield stress of most metals decrease with the rise of temperature whereas the density decreases due to thermal strains. Therefore, the temperature field influences the plasticity and hence the cutting process. Because of the shape of the work-piece changes, it should be noted that, within the large deformation and the

cutting process the heat conduction equation is a function of the deformation. The flow chart of the present work is shown in Fig. 1.

5 Hysteresis energy analysis

Hysteresis is the time-based dependence of a system output between loading and unloading condition. The hysteresis loop occurs when there is a difference between the input and output state of loading. However, this surrounding area can be calculated as hysteresis energy. In the laser cutting process, the power distribution and cutting efficiency can be evaluated from the general energy balance in the cutting section, which is described by Powell et al. [25] in the following equation:

$$E_{in} = E_{cut} + (E_{tran} + E_{refl} + E_{cond} + E_{rad}). \quad (12)$$

Or supplied energy to the cut region = Energy loss from cut region + Cutting energy

All the energy losses are from the cut region, excluding E_{cut} and E_{in}, that are more separated into primary and secondary loss [26]. The dissipated energy from radiation of laser beam is transferred internally and externally that it is part of primary energy loss. It is hard to estimate primary losses hypothetically, but it is possible experimentally. When the laser beam passed the cutting region in a straight way, the internal reflection would be released in the same direction. The secondary energy loss including the radiation, convection and conduction. The coduction secondary energy loss is dominate in compare to the radiation and convection. Because of this reason,the role of radiation and convection can be neglected in order to evaluate the secondary energy loss. In addition, due to the small size of HAZ in comparison with the cutting area this assumption is acceptable [27]. The E_{cut} in Eq. 12 is the result of energy needed to eliminate a material unit volume from the cut region as

$$E_v = \rho c(T - T_0) + \rho C_v. \quad (13)$$

Thus, the cut energy is equal to

$$E_{cut} = E_{loss}. \quad (14)$$

E_{loss} is divided into primary and secondary parts. In addition, by assuming that, the radiation and convection are negligible and secondary losses are merely conductive [26]. However, In this case, the conductive energy is simply expressed as

$$E_{cond} = E_{cut} - E_{loss}. \quad (15)$$

A materials power absorption efficiency η indicates the amount of absorbed energy at the cut region that is defined as

$$\eta = \frac{E_{in} - E_{loss}}{E_{in}} = 1 - \frac{E_{loss}}{E_{in}}. \quad (16)$$

Furthermore, cutting efficiency may be defined as a ratio of required energy to cut to the delivered energy to the cut area:

$$C_{eff} = \frac{E_{cut}}{E_{in}}. \quad (17)$$

In the present study, the calculated hysteresis energy H can be used as an alternative method to estimate the efficiency of cutting process. Since, hysteresis energy is defined as the differences between total energy E_{in} and consumed energy E_{cut} and also gives a direct indication for the cutting process quality. Therefore, $E_{loss} = H$ and the cutting and power absorption efficiencies can be calculated. The smaller magnitude of H goes to obtain to the small amount of residual stress and energy loss. In addition, E_{cut} and H can be calculated by the FE model as well. Therefore, the is simply expressed as;

$$\eta = 1 - \frac{H}{E_{in}}. \quad (18)$$

6 Finite element model

To simulate the laser cutting process, a solid three-dimensional model was generated. To produce the heat flux of laser beam,

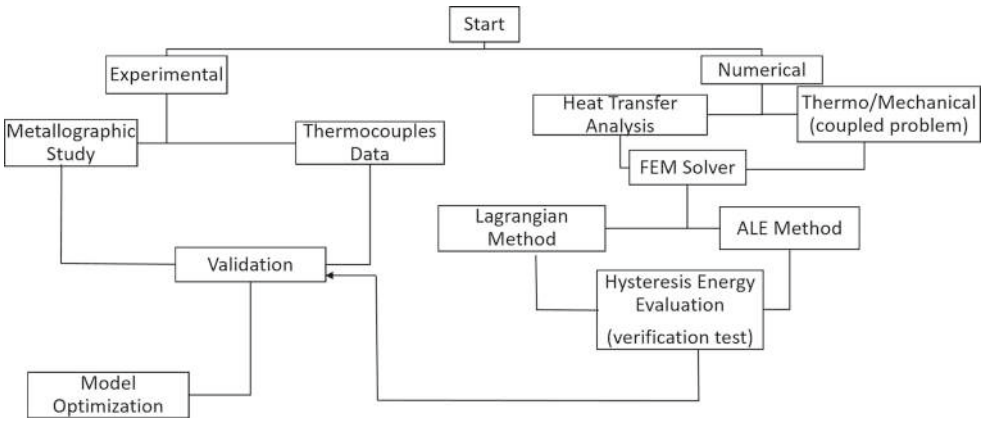

Fig. 1 Flow chart of the research work

a FORTRAN-based computer code was implemented in ABAQUS user-defined subroutine. Having reached to the thermal stress, a coupled analysis was applied for mapping the thermal stress to the mechanical stress. The continuum damage model was used to remove element from cutting path during laser induction. The energy balance analysis was performed to evaluate the hysteresis energy. Two different FE formulations: Lagrangian and ALE methods were used to compare with experimental data in order to attain more reliable simulation results.

6.1 Model of the work-piece

The work-piece is modeled as a sheet plate in 3D format. The schematic view of FE model used for simulating with the general dimension and the coordinate system as well as applied boundary conditions is shown in Fig. 2. In the current analysis, the laser is applied as a moving source in positive Y-direction with fixed specimen in order to ease numerical implementation.

6.2 Material properties and failure criterion

In this study, the work-piece is modeled as elastic-plastic material with a yield stress that alters by temperature and isotropic hardening. If the thermal load exceeds yield limit, some part of material will remain in plastic form when the load is removed. The properties of used aluminum sample in this study are presented in Table 1.

The continuum damage mechanism was used to model the material degradation and subsequently element removal. When the material is subjected to the elevated temperature, the elastic modules and the plastic stress will be decreased until reaching to the corresponding fracture strain. Material failure refers to the complete loss of load-carrying capacity those results from progressive degradation of the material stiffness. In this work, the failure criterion based on ductile damaged model is introduced. However, a simple empirical critical magnitude as strain fracture function is defined

Table 1 Aluminum sample's thermo-mechanical properties [28]

T (K)	Cp (J/kg K)	K (W/mk)	E (GPa)	α $(1/k.10^{-}5)$	Yield stress (MPa)
300	470	164	72.4	0.270	473
500	521	194	63.5	0.274	293
700	773	210	56.1	0.277	150
770	800	220	50	0.283	100

as the ductile damage, $\epsilon_d = 0.02821/\left(\epsilon^{0.3131}\Delta T_B{}^{0.8638}\right)$ where ΔT_B represents brittle temperature range [29].

6.3 Applied load and boundary condition

Laser heat flux by Gauss distribution and prescribed velocity of 15 mm/s along the positive Y-axis through user subroutine DFLUX applied to the thermal model. At first, the thermal analysis is solved to obtain the temperature field throughout the specimen as a function of time which is then provided as an input for the stress analysis to determine the thermal stress and energy fields in close to the laser cutting section. In this simulation, to avoid rigid motion body problem, one point was fixed in all DoF and the left edge was constrained in x direction U_x =0 (see Fig. 2).

6.4 Meshing method and element type

Figure 3 illustrates the Lagrangian computational mesh and its related nodes that they follow the associated material points during applying load. In Lagrangian method, the solution domain will be fixed that it would be appropriate for structural analysis. However, when the structure is subjected to the large deformation or element removal the source of remeshing operation will be neglected. On the other hand, in ALE method, the nodes of solution domain may be moved with the continuum in conventional Lagrangian manner or can be maintain fixed as Eulerian formulation. Moreover, it can be moved arbitrarily in some

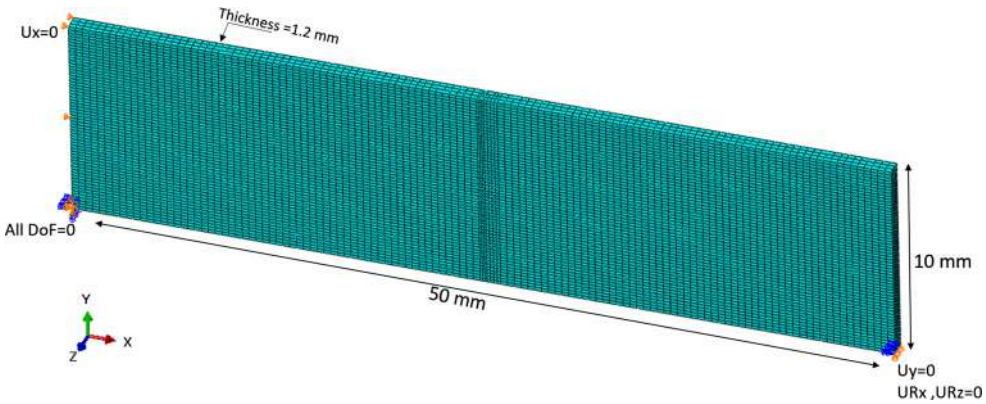

Fig. 2 Schematic view of FE model and the coordinate system along with the boundary conditions

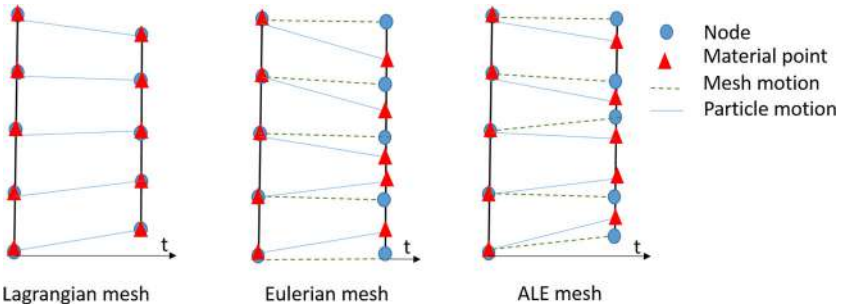

Fig. 3 presentation of Lagrangian, Eulerian ans ALE meshing in a 1D structure

specified ways to provide the ability of continues rezoning. Due to this degree of freedom, the ALE method is capable to handle greater distortion than Lagrangian technique [30].

Figure 4 indicates the schematic view of ALE method for one-dimensional structure. Through this formulation, a high-quality mesh can be maintained throughout the analysis by allowing free mesh movement, even if large material loss or deformation of material happens. Once the critical regions are identified in the geometry, the mesh is developed. The critical regions are considered as the regions where high temperature gradient and strain occur during the laser inducing. These regions are the high-density element area around the heat-affected zone and the laser beam path. Therefore, as it mentioned before, the refined mesh is selected in this region in order to capture the temperature and stress fields with high resolution as well. Continuum, three-dimensional 8-node linear heat transfer elements (C3D8R) are used in the thermal analysis whereas for stress analysis, three-dimensional 8-nodelinear stress elements (C3D8R) are used as Lagrangian method in the first step and then the ALE formulation is used in second attempt.

6.5 Simulation procedure

The corresponding displacement from thermal analysis was taken into account as a solution variable at the nodal coordinate, and boundary and loading conditions were transferred to the next step of coupled simulation . The stress-strain increments can be calculated at any point inside the component through the interpolation functions using the constitutive and compatibility equations. A total thermal strain coefficient dependent on temperature $\alpha'(T)$ is used. The total thermal expansion and differential coefficients are connected to each other via:

$$\alpha'(T) = \frac{1}{T - T^0} \int_{T^0}^{T} \alpha(T) dt \tag{19}$$

where $\alpha(T)$ is the coefcient of thermal expansion dependent on temperature and T^0 is a reference temperature defining the area that the material has no dilatational strain (in the current problem, assumed as the mechanical coherency temperature). After inducing the thermal flux the stress analysis was performed on the geometry regarding updated boundary condition. In this step, the damage-based mechanism is activated and the material will be removed after passing the fracture strain threshold.

7 Experimental procedure

In this study, a carbon dioxide laser cutting machine with variable frequencies to irradiate the surface of work-piece and 1.6 kW delivering nominal output power (see Fig. 5). The intensity of laser output is Gaussian, with 127 mm nominal focal length of the focusing lens.

A single pass was performed to create the cut. In the irradiated region, the incident beam absorption is reduced by the surface reflectivity. Yet, the reflectivity decreases when the melting temperature is achieved [31] and the incident power becomes sufficient for single-pass cut of aluminum alloy. For validating the predictions of temperature

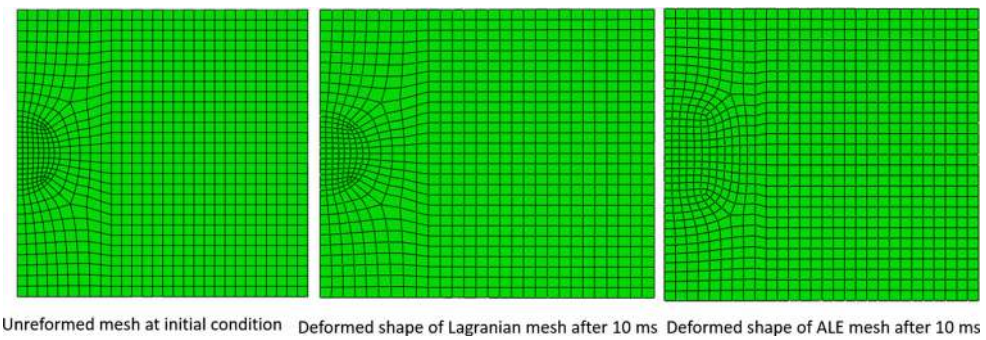

Fig. 4 comparison between Lagrangian and ALE meshing for a structure subjected to the axial loading after 10 ms

Fig. 5 Photo of the experimental setup of the laser cutting and thermocouples location

variation, the temporal variation of surface temperature was monitored by using two thermocouples at the region 1 mm far from the laser induced path, as shown in Fig. 5 . The field emission scanning electron microscope (FESEM) was used to perform morphology analysis in cutting surface.

8 Results and discussion

8.1 Surface temperature and balance efficiency

Laser cutting of aluminum sheets was carried out, and temperature, stress, and energy analysis by using the FEM was analyzed and was compared with the experimental results. FESEM analysis was done for morphological and metallurgical changes of the cutting surface. Laser cutting process has two main factors to reach the high efficiency named "power of the laser" and "cutting speed" [4, 32]. In order to obtain the higher efficiency, the balance between laser power and cutting speed is needed. Figure 6 shows that by increasing the cutting speed more power should be used to reach the melting temperature in HAZ. However, reduction of cutting speed helps to accelerate heat saturation at the cutting area. On the other hand, reduction of cutting speed can increase the temperature at HAZ that can be influence on the neighborly elements behavior. Therefore, the most efficiency balance between laser power and cutting speed in this study yielded to 1.6 (kW) and 15.33 (mm/s) respectively. As the graph shows, the maximum temperature for these characterized magnitude increased through the line based on conduction phenomena and after 4 mm distance from start point it remains approximately constant.

Figure 7 shows contour plots for the predicted temperature variations of the laser cutting for aluminum sheets. It can be seen that the temperature is uniform across the thickness of the sheets and increases in regions where the laser spot is located. The temperature decay is gradual during lighted spot focal point and it becomes sharp as laser scan goes far away from the work-piece edges. This conduct technique may be attributed to laser beam intensity distribution at the surface, which would Gaussian and the volumetric absorption of laser beam in substrate material as well.

8.2 Surface temperature along the line of cut

Figure 8 reveals to prediction of surface temperature variety along y-direction and thermocouples data got from the work-piece in the same area. It can be observed that both findings are in good agreement and the contrasts between both outcomes are within the experiment error, which is in order of 8%. The estimated error could be related to the some local non-isotropy in the microstructure or laser beam fluctuation during the process.

The prediction of surface temperature versus historical time for seven different locations at the working cross-area of the sheet in symmetric format is shown in Fig. 9. It shows the assumption of the isotropic properties have well agreement. The heat conduction from the cut section to its neighbors becomes less because of the small area

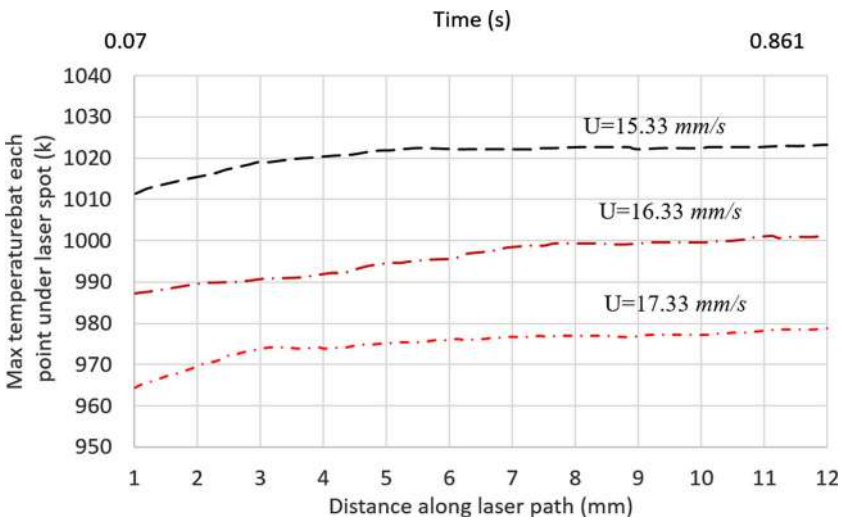

Fig. 6 Effect of laser cutting speed over time to reach steady temperature

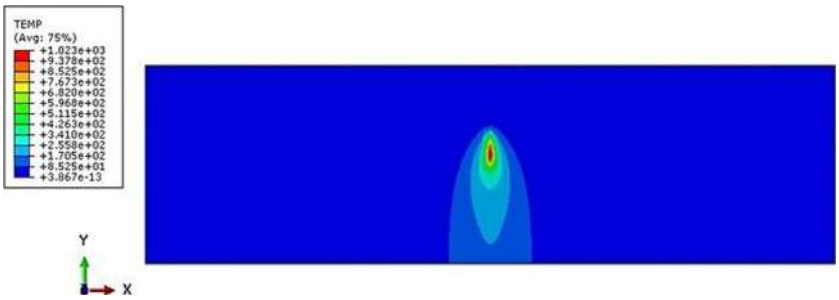

Fig. 7 Temperature distribution of laser cutting for aluminum sheets

surrounding the cutting section. In addition, it can clearly be seen that the temperature variation for different time spot go far away from the cut line and the temperature decreased and it is symmetry due to geometry of the work-piece. It is worth mentioning that the temperature remains high in the area where the laser power has passed after cutting completion. When the temperature reaches to peak that is higher than the liquids temperature (911K), the phase changing in the FE user subroutine was taken into account. This step will be remained until material evaporation.

8.3 Hysteresis energy

Hysteresis energy is an important criterion to validate the simulation technique as already discussed. To get an appropriate result, the difference between total energy and consumed energy should be less than 10% [26, 33]. Figure 10 shows the variation in the hysteresis energy differences for two different methods. The graph clearly illustrates that the magnitude of hysteresis energy in ALE method is less than the Lagrangian method for whole simulation process.

Hysteresis energy accumulated in the work-piece after cutting process. Although the hysteresis energy remained in the model with Lagrangian mesh is not acceptable. In this study, energy balance comparison shows that the ALE formulation is more reliable when the material removal is one of the simulation goal. Based on Eqs. 17 and 18, the power absorption and cutting efficiency for Lagrangian and ALE method are derived and shown in Fig. 11. As the graph shows, the energy absorptivity increased as the distance along the laser induced process increased. In terms of energy balance, it can be clearly seen that, although the efficiency of power absorption in Lagrangian method is bigger than the ALE method, but the cutting efficiency is less while with less magnitude of power absorption, the cutting process in ALE method has a better efficiency. In a better word, in the ALE method, the efficiency of cutting process is better by using less magnitude of power input.

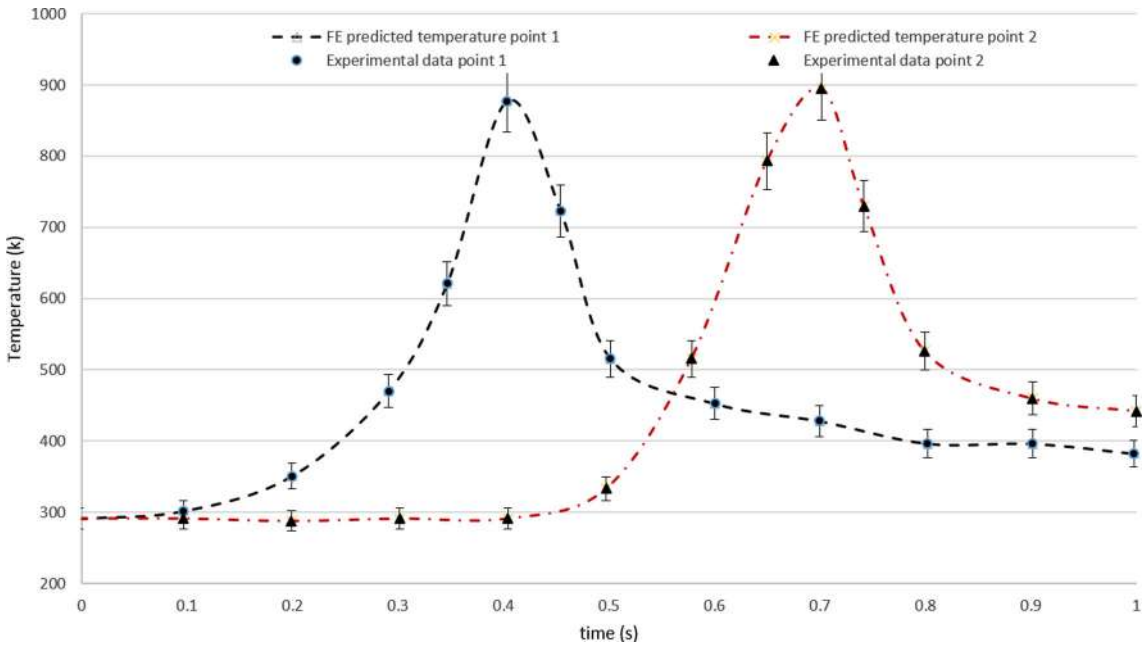

Fig. 8 Comparison of surface temperature derived from simulation and thermocouples data at 1 mm away from cut edge

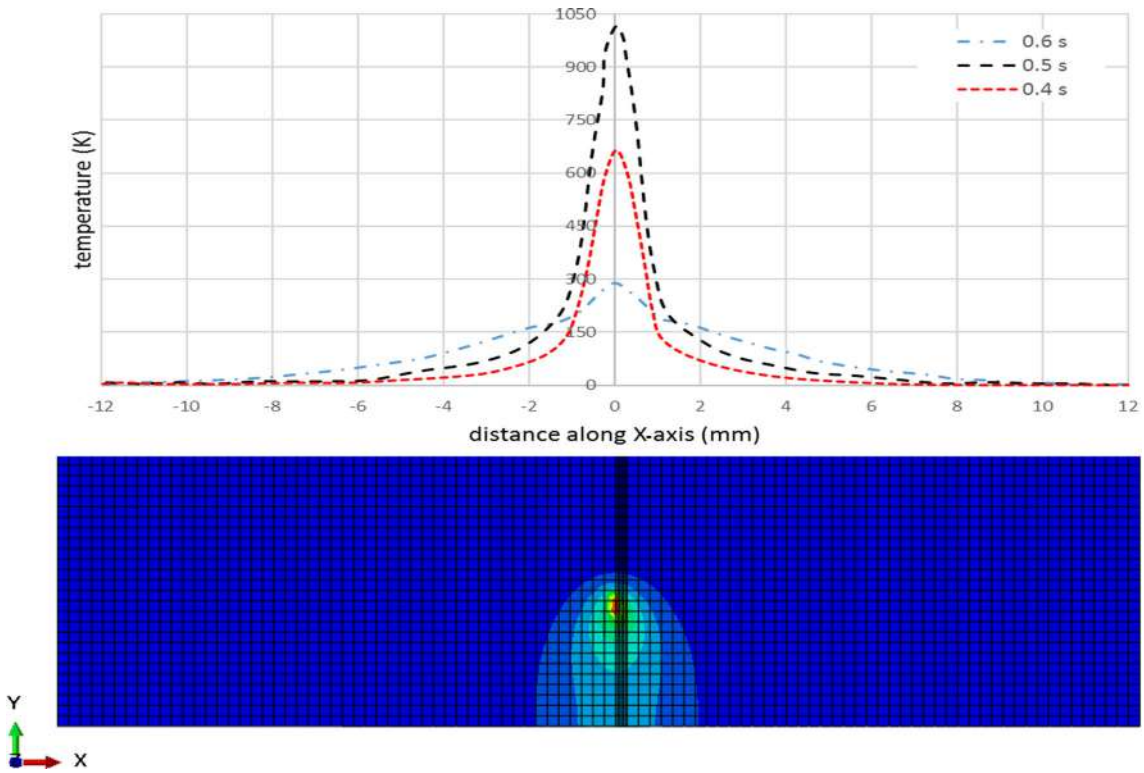

Fig. 9 Temperature variations along x-axis for different times at the middle cross section of sheet

Therefore, based on the result of ALE model, this model is more efficient to simulate laser-cutting process regarding the energy criterion and the thermal analysis results. Therefore, it is suggested that the energy balance in the simulation should be evaluated in order to obtain the reliable results in compare to the real process of laser cutting.

8.4 Von misses stress and Kerf width

Figure 12 shows the von Misses stress results of two different FE formulations through the work-piece after finishing the laser cutting process of aluminum sheet. Fig. 12a shows the cut work-piece which is simulated by the

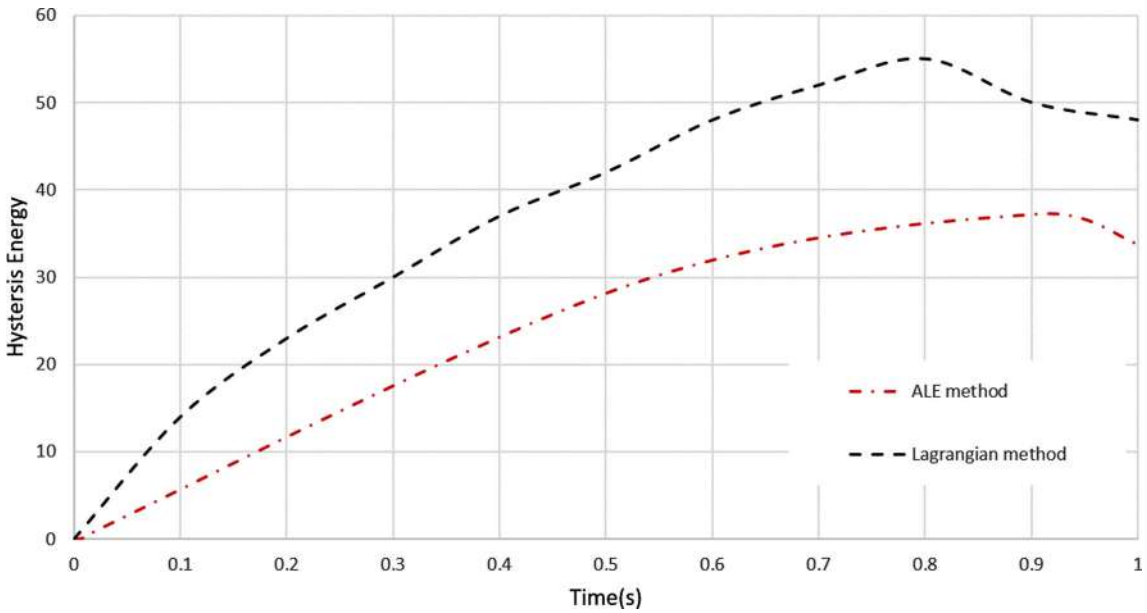

Fig. 10 Hysteresis energy based on two different FE-simulation methods

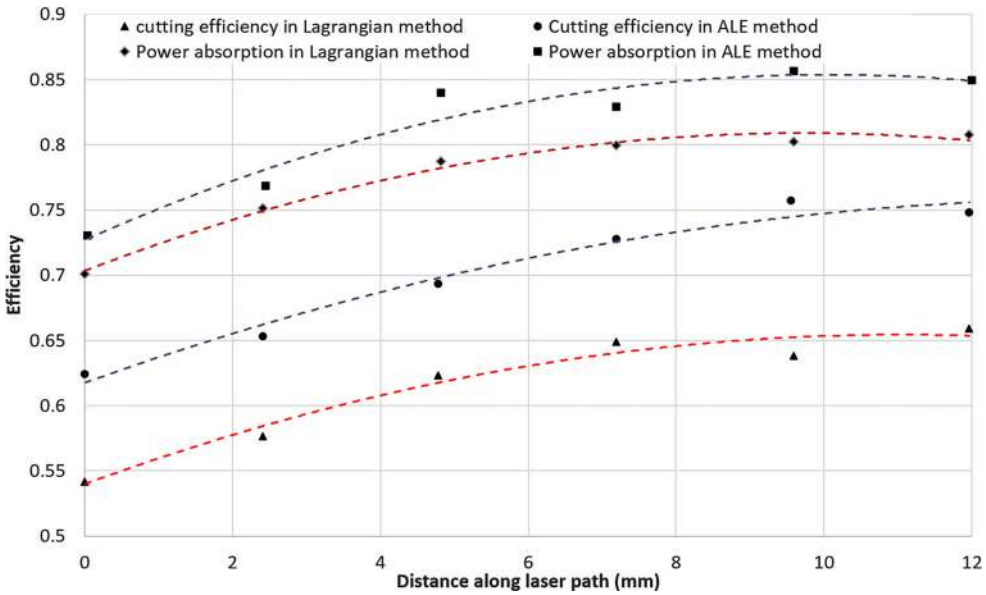

Fig. 11 Cutting and power absorption efficiency based on two different methods

Lagrangian mesh whereas, Fig. 12b is the cut sample with ALE method after finishing the process and the failure criterion.

Figure 13 compare the removed element and the kerf width of (a) Lagrangian method and (b) ALE method with (c) experimental observation. The figure illustrate that after cutting process, the kerf width value is around 0.12, 0.13, and 0.16 mm for experimental, ALE, and Lagrangian methods, respectively. Therefore, it can be said that the ALE method results are more accurate than Lagrangian method. To depict the cutting zone in mentioned figure, the additional area in length of the specimen is cropped.

Figure 14 shows the von Misses stress distribution for two different FE techniques. The time history and path line to extract the stress contour for von Misses stress distribution are similar to those shown in Fig. 9 Since the middle cutting zones of the sheets are not free to expand, they cause high stress level generated in these regions. Von Misses stress reach high values in the area where the gradient of temperature is high which occurs in neighboring element to the irradiated spot edges. Therefore, the maximum stress occurs at the middle of specimen close to the cutting path. Moreover, after finishing the simulation at the middle of the work-piece on the cutting line, due to element removal, the stress value becomes zero. When comparing the von Misses stress levels due to two different simulation methods, the magnitude of the stress which extracted by using the Lagrangian mesh at the peak point is around 281MPa whereas this magnitude is around 230MPa when ALE model is performed. Therefore, it means that the residual stress, which is remained in the work-piece in ALE model, is less than conventional Lagrangian model.

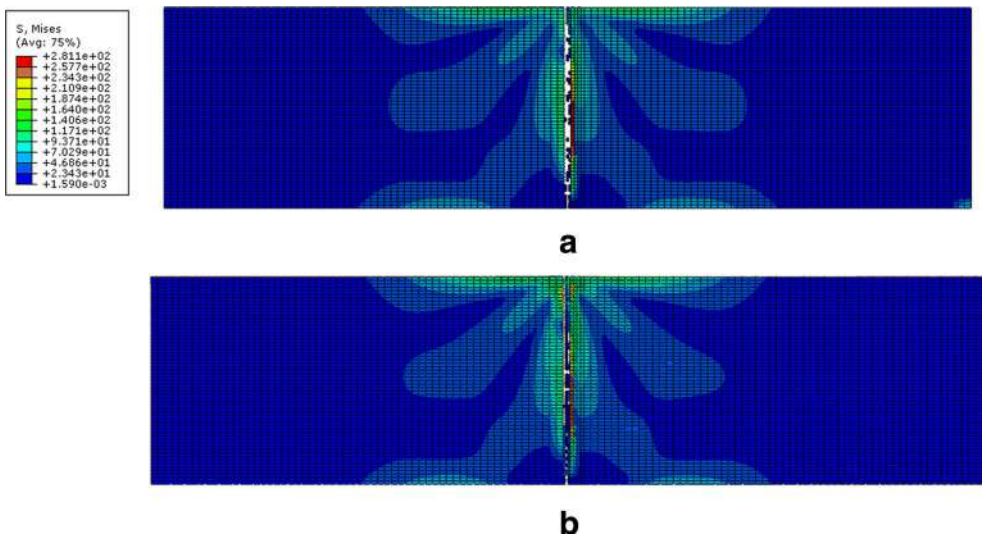

Fig. 12 The von Misses stress contours for Lagrangian (**a**) and ALE (**b**) method

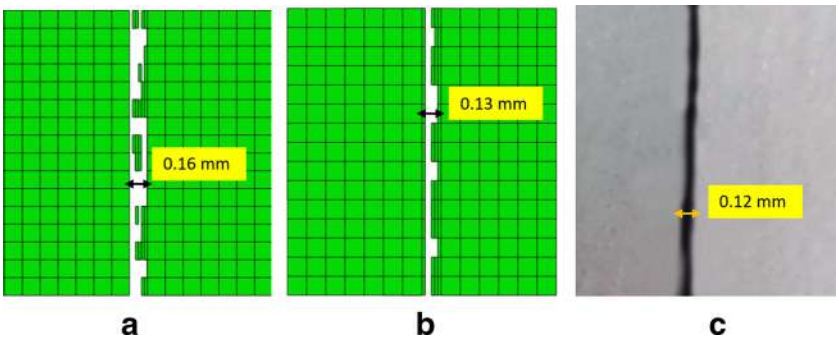

Fig. 13 The kerf width comparison for Lagrangian (**a**) ALE (**b**) and (**c**) real experiment

In general, the von Misses stress reaches low values by using ALE model. In another word, the more precise calculated residual stress can be reached by using ALE method. However, the von Misses stress becomes high next to the region of cutting zone; but as the graphs show, the magnitude of stress in ALE method in different times are approximately constant and shows the same magnitude. In addition, it is so important to mention that, the HAZ for two different methods are specified with dash line due to the stress distribution. The results show that the

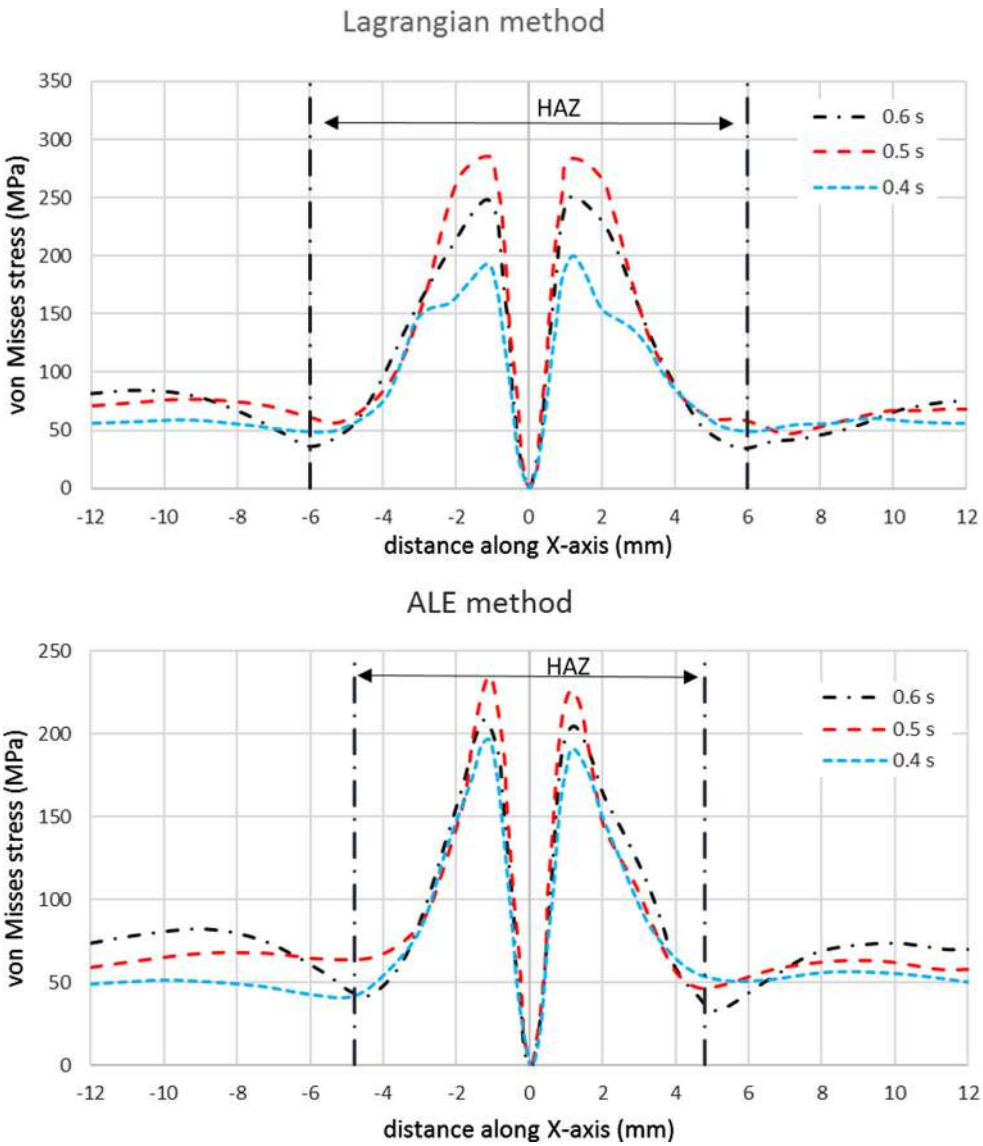

Fig. 14 The von Misses stress distribution in the transverse direction (X-axis) for two different method analysis

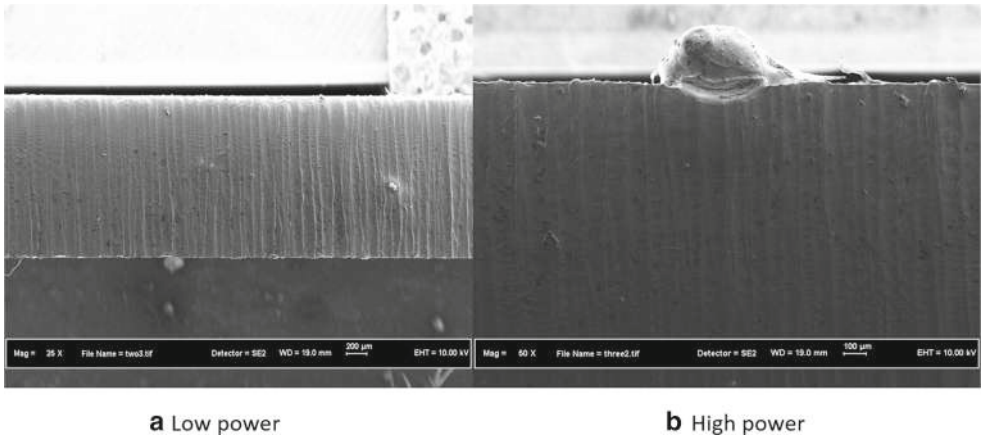

Fig. 15 FESEM micrographs of laser cutting process for comparison of different laser power

HAZ in ALE method is smaller than Lagrangian method and it can be interpreted that how kerf width of the ALE method in Fig. 13b is uniform and smaller than Lagrangian method.

8.5 Cut surface quality

Figure 15 shows the FESEM micrograph of the laser-cutting surface. It can be seen that the most efficient condition that extracted from experimental test (see Fig. 6), yields to a cut surface that is free from any dross attachments and cracks (Fig. 15a). On the other hand, by increasing the power of the laser the dross attachment created at the cut edge (Fig. 15b). It is important to mention that dross attachment is usually appears on cutting surfaces [34]. It is connected with the effect of cooling gas on viscosity of molten material. It is obvious that by reducing the temperature, the viscosity of the molten material increased. Beside the power of the laser, the cutting speed has an important role in laser cutting process.

Figure 16 clearly illustrates the effect of cutting speed on the laser cutting process for normal (a) and high speed (b) process. It shows that, although the process of laser cutting is the rapid one, but the sufficient consideration needed to prevent the destructive effects such as crack, voids, or cavities in cutting surface. The FESEM micrographs show that the forming of striations is different at the bottom surface and the dross attachments observed in this region is associated with instability of the molten material which flows during the cutting process which is caused by the high speed machining.

XRD analysis (Fig. 17) illustrates the chemical composition after cutting process. The first spectrum (a) as the best machining condition (1.6 (kW) and 15.33 (mm/s)) shows that the dominate element was aluminum and the observed carbon from cutting process was infinitesimal. In the second spectrum (b), it can be seen that the substrate aluminum alloy has been chemical decomposed into different elements and the magnitude of carbon shows that the temperature was high at this region.

The XRD element analysis of laser cut section shows in Table 2. By comparison between the atomic and weight percentage value, it is found that the effect of laser power on decomposition phenomena and generally the efficiency of

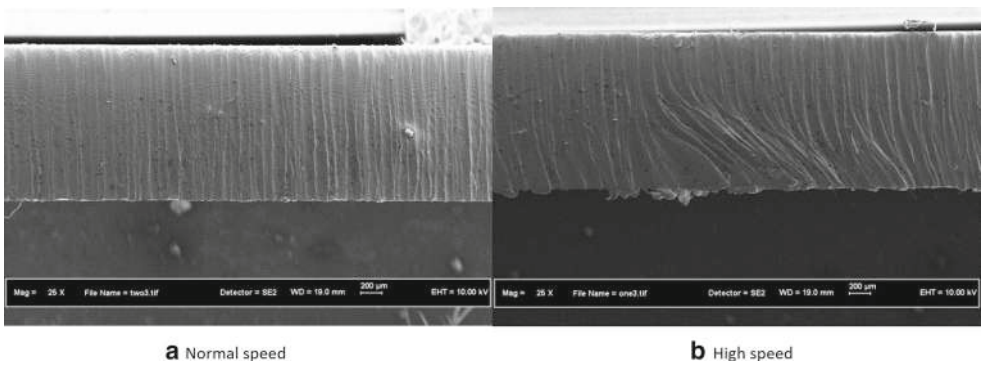

Fig. 16 FESEM micrographs of laser cutting process for comparison of different cutting speed

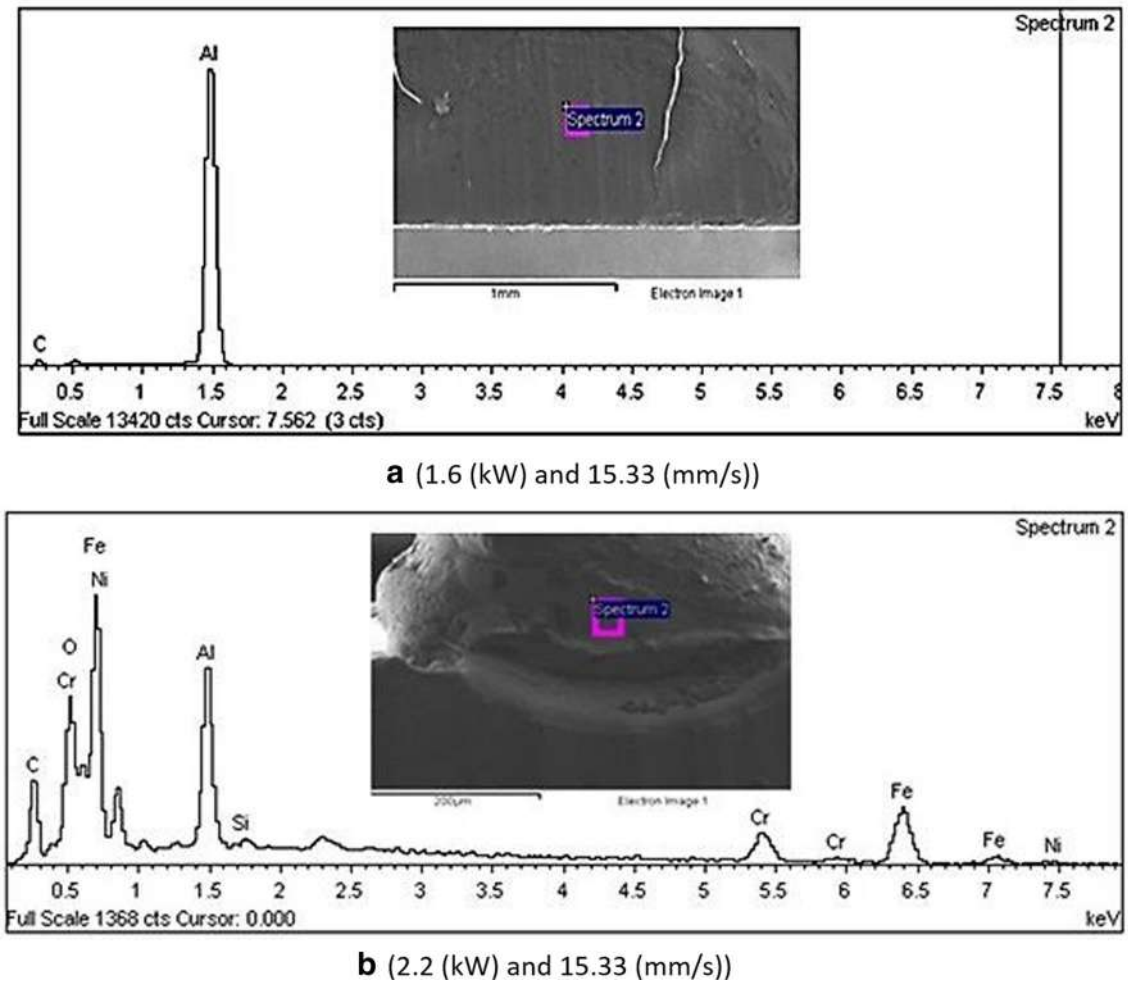

Fig. 17 X-ray diffraction composition analysis for the laser cut section

Table 2 XRD results obtained at the cutting surface

Element	App *Conc*	Intensity *Corrn*	Weight %	Weight Sigma %	Atomic %	Cutting condition
C K	0.08	0.3633	13.77	0.88	25.4	Normal
Al K	1.81	1.3126	86.23	0.88	74.6	Normal
C K	0.09	0.3641	13.97	0.9	26.73	High speed
Al K	1.96	1.312	86.03	0.9	73.27	High speed
C K	0.11	0.8185	8.43	0.66	28.65	High power
O K	0.19	2.0872	5.66	0.43	12.92	High power
Al K	0.11	0.9925	6.8	0.39	9.21	High power
Si K	0	1.0297	0.23	0.14	0.3	High power
Cr L	0.18	0.7752	13.91	3.48	9.77	High power
Fe L	0.62	0.7042	54.11	2.47	32.39	High power
Ni L	0.08	0.4654	10.87	0.97	6.76	High power

the cutting process is more considerable than the speed of the laser. It is attributed to the effect of high temperature on aluminum alloy which chemical decomposed take place in this region.

9 Conclusion

Laser cutting of aluminum sheets with 1.2 mm thickness has been studied numerically and experimentally. Temperature variation and thermal stress induced during the cutting process were predicted by two different finite element techniques. Predicted surface temperature is validated via experimental data. Elemental and morphological changes examined by using field emission scanning electron microscope and chemical composition of the substrate material have been also analyzed. The simulation results clearly illustrated the effectiveness of FE formulation on the predicted goal values. It is found that the calculated temperature exceeded the liquids temperature of substrate material at cutting section; therefore, super warming from claiming fluid stage happened in this region. The thermal stresses reached high values at the middle of the work-piece close to the cut line since temperature gradient is high and the material is not totally free to expand. The striation patterns were formed at cutting surface when the speed rate is high whereas dross attachments and change chemical decomposition were observed at high power laser. The suggested energy balance evaluation could be a good tool to verify the accuracy of the numerical solution. Studying the effects of laser power and cutting speed on the process efficiency revealed that the ALE method is in well agreement with experimental results. In general, the ALE method is more reliable to predict the laser cutting process in comparison with the conventional Lagrangian method.

References

1. Roessler DM (1990) Detroit looks to lasers. Mech Eng-CIME 112:38–46
2. Lawson W (1986) Laser cutting of composites, Society of Manufacturing Engineers, Conference on Composites in Manufacturing, 5 th, Los Angeles, CA, 1986
3. Keikhosravy M, Hashemi Oskouei R, Soltani P, Atas A, Soutis C (2012) Effect of geometric parameters on the stress distribution in Al 2024-T3 single-lap bolted joints. Int J Struct Integr 3(1): 79–93
4. Sharma A, Yadava V (2012) Modelling and optimization of cut quality during pulsed Nd: YAG Laser cutting of thin Al-alloy sheet for straight profile. Opt Laser Technol 44(1):159–168
5. Kim MJ, Majumdar P (1995) Computational model for high-energy laser-cutting process. Numer Heat Transfer, Part A: Appl 27(6):717–733
6. Eltawahni HA, Hagino M, Benyounis KY, Inoue T, Olabi A-G (2012) Effect of CO 2 laser cutting process parameters on edge quality and operating cost of AISI316l. Opt Laser Technol 44(4):1068–1082
7. Stournaras A, Stavropoulos P, Salonitis K, Chryssolouris G (2009) An investigation of quality in CO 2 laser cutting of aluminum. CIRP J Manuf Sci Technol 2(1):61–69
8. Wang Y, Wang X, Kang R, Xu W, Guo D (2012) Experimental study on laser cutting based on removal forms for aluminum alloy sheet, Zhongguo Jiguang(Chinese journal of lasers), 39, 8 0803007–7
9. Anthony TR, Cline HE (1977) Surface rippling induced by surface-tension gradients during laser surface melting and alloying. J Appl Phys 48(9):3888–3894
10. Pandey AK, Dubey AK (2013) Multiple quality optimization in laser cutting of difficult-to-laser-cut material using grey–fuzzy methodology. Int J Adv Manuf Technol 65(1–4):421–431
11. Dubey AK, Norkey G, Agrawal S (2012) Parameter optimisation in laser cutting of aluminium alloy sheet. Int J Mechatronics Manuf Syst 5(3-4):179–188
12. Sheng PS, Joshi VS (1995) Analysis of heat-affected zone formation for laser cutting of stainless steel. J Mater Process Technol 53(3):879–892
13. Yilbas BS, Akhtar S, Karatas C (2012) Laser straight cutting of alumina tiles: thermal stress analysis. Int J Adv Manuf Technol 58(9-12):1019–1030
14. Yilbas BS, Akhtar S, Keles O (2014) Laser cutting of triangular blanks from thick aluminum foam plate: Thermal stress analysis and morphology. Appl Therm Eng 62(1):28–36
15. Yi P, Liu Y, Shi Y, Jang H, Lun G (2011) Effects analysis of ambient conditions on process of laser surface melting. Opt Laser Technol 43(8):1411–1419
16. Anderson MC, Shin YC (2006) Laser-assisted machining of an austenitic stainless steel: P550. Proc Inst Mech Eng B J Eng Manuf 220(12):2055–2067
17. Fu CH, Sealy MP, Guo YB, Wei XT (2015) Finite element simulation and experimental validation of pulsed laser cutting of nitinol. J Manuf Process 19:81–86
18. Sharma P, Dubey AK, Pandey AK (2014) Numerical study of temperature and stress fields in laser cutting of aluminium alloy sheet. Procedia Mater Sci 5:1887–1896
19. Kardas OO, Keles O, Akhtar S, Yilbas BS (2014) Laser cutting of rectangular geometry in 2024 aluminum alloy: Thermal stress analysis. Opt Laser Technol 64:247–256
20. Donea J, Huerta A (2003) Finite element methods for flow problems, John Wiley & Sons
21. (2012). Systèmes, Dassault, Abaqus v6. 12 Documentation-ABAQUS analysis users manual, Abaqus, Providence RI
22. Mase GT, Smelser RE, Mase GE (2009) Continuum mechanics for engineers, CRC press
23. Hibbitt K (2001) Sorensen ABAQUS/explicit Users Manual
24. Glaser S, Kröplin B (1991) Thermo Mechanical Coupling in Elasto-Plastic Analysis, The finite element method in the 1990s, 59–67 Springer
25. Ivarson A, Magnusson C, Powell J (1994) An energy balance for inert gas laser cutting. Laser Mater Process 2306:12
26. Ng SL, Lum KCP, Black I (2000) CO 2 Laser cutting of MDF: 2. Estimation of power distribution. Opt Laser Technol 32(1): 77–87

27. Chien CY, Gupta MC (2005) Pulse width effect in ultrafast laser processing of materials. Appl Phys A 81(6):1257–1263
28. Ogden RW, Roxburgh DG (1999) A pseudo–elastic model for the Mullins effect in filled rubber, Proc R Soc Lond A: Math, Phys Eng Sci, 455, 1988, 2861–2877, The royal society
29. Li C, Thomas BG (2004) Thermomechanical finite-element model of shell behavior in continuous casting of steel. Metall Mater Trans B 35(6):1151–1172
30. Donea J, Huerta A, Ponthot J-P, Rodriguez-Ferran A (2004) Encyclopedia of computational mechanics vol. 1 fundamentals. Chapter 14: Arbitrary Lagrangian-Eulerian methods
31. Ctibor P, Kraus L, Tuominen J, Vuoristo P, Chraska P (2007) Improvement of mechanical properties of alumina and zirconia plasma sprayed coatings induced by laser post-treatment. Ceram Silik 51(4):181
32. Scintilla LD, Tricarico L (2013) Fusion cutting of aluminum, magnesium, and titanium alloys using high-power fiber laser. Opt Eng 52(7):076115–076115
33. Kim MJ (2000) Transient evaporative laser-cutting with boundary element method. Appl Math Model 25(1):25–39
34. Yilbas BS, Akhtar S, Karatas C (2014) Laser cutting of triangular geometry into alumina tiles: morphological changes and thermal stress analysis. Mach Sci Technol 18(3):424–447

Terms and Conditions

Springer Nature journal content, brought to you courtesy of Springer Nature Customer Service Center GmbH (“Springer Nature”).
Springer Nature supports a reasonable amount of sharing of research papers by authors, subscribers and authorised users (“Users”), for small-scale personal, non-commercial use provided that all copyright, trade and service marks and other proprietary notices are maintained. By accessing, sharing, receiving or otherwise using the Springer Nature journal content you agree to these terms of use (“Terms”). For these purposes, Springer Nature considers academic use (by researchers and students) to be non-commercial.
These Terms are supplementary and will apply in addition to any applicable website terms and conditions, a relevant site licence or a personal subscription. These Terms will prevail over any conflict or ambiguity with regards to the relevant terms, a site licence or a personal subscription (to the extent of the conflict or ambiguity only). For Creative Commons-licensed articles, the terms of the Creative Commons license used will apply.
We collect and use personal data to provide access to the Springer Nature journal content. We may also use these personal data internally within ResearchGate and Springer Nature and as agreed share it, in an anonymised way, for purposes of tracking, analysis and reporting. We will not otherwise disclose your personal data outside the ResearchGate or the Springer Nature group of companies unless we have your permission as detailed in the Privacy Policy.
While Users may use the Springer Nature journal content for small scale, personal non-commercial use, it is important to note that Users may not:

1. use such content for the purpose of providing other users with access on a regular or large scale basis or as a means to circumvent access control;
2. use such content where to do so would be considered a criminal or statutory offence in any jurisdiction, or gives rise to civil liability, or is otherwise unlawful;
3. falsely or misleadingly imply or suggest endorsement, approval , sponsorship, or association unless explicitly agreed to by Springer Nature in writing;
4. use bots or other automated methods to access the content or redirect messages
5. override any security feature or exclusionary protocol; or
6. share the content in order to create substitute for Springer Nature products or services or a systematic database of Springer Nature journal content.

In line with the restriction against commercial use, Springer Nature does not permit the creation of a product or service that creates revenue, royalties, rent or income from our content or its inclusion as part of a paid for service or for other commercial gain. Springer Nature journal content cannot be used for inter-library loans and librarians may not upload Springer Nature journal content on a large scale into their, or any other, institutional repository.
These terms of use are reviewed regularly and may be amended at any time. Springer Nature is not obligated to publish any information or content on this website and may remove it or features or functionality at our sole discretion, at any time with or without notice. Springer Nature may revoke this licence to you at any time and remove access to any copies of the Springer Nature journal content which have been saved.
To the fullest extent permitted by law, Springer Nature makes no warranties, representations or guarantees to Users, either express or implied with respect to the Springer nature journal content and all parties disclaim and waive any implied warranties or warranties imposed by law, including merchantability or fitness for any particular purpose.
Please note that these rights do not automatically extend to content, data or other material published by Springer Nature that may be licensed from third parties.
If you would like to use or distribute our Springer Nature journal content to a wider audience or on a regular basis or in any other manner not expressly permitted by these Terms, please contact Springer Nature at

onlineservice@springernature.com